# Highly deformed <sup>40</sup>Ca configurations in <sup>28</sup>Si + <sup>12</sup>C

M. Rousseau\*, C. Beck, C. Bhattacharya<sup>†</sup>, V. Rauch, O. Dorvaux, K. Eddahbi, C. Enaux, R.M. Freeman, F. Haas, D. Mahboub<sup>‡</sup>, R. Nouicer<sup>§</sup>, P. Papka, O. Stezowski\*\*, and S. Szilner

Institut de Recherches Subatomiques, UMR7500, Institut National de Physique Nucléaire et de Physique des Particules - Centre National de la Recherche Scientifique/Université Louis Pasteur, 23 rue du Loess, B.P. 28, F-67037 Strasbourg Cedex 2, France

### A. Hachem and E. Martin

Université de Nice-Sophia Antipolis, F-06108 Nice, France

# S.J. Sanders and A.K. Dummer<sup>††</sup>

Department of Physics and Astronomy, University of Kansas, Lawrence, Kansas 66045, USA

### A. Szanto de Toledo

Departamento de Física Nuclear, Instituto de Física da Universidade de São Paulo, C.P.

66318-05315-970 - São Paulo, Brazil

(October 27, 2018)

<sup>\*</sup>Corresponding author. Electronic address: marc.rousseau@ires.in2p3.fr

<sup>&</sup>lt;sup>†</sup>Permanent address: VECC, 1/AF Bidhan Nagar, Kolkata 64, India.

<sup>&</sup>lt;sup>‡</sup>Present address: University of Surrey, Guildford GU2 7XH, United Kingdom.

<sup>§</sup>Present address: Department of Physics, University of Illinois at Chicago, Chicago, Illinois 60607-7059, USA.

<sup>\*\*</sup>Permanent address: IPN Lyon, F-69622 Villeurbanne, France.

<sup>&</sup>lt;sup>††</sup>Present address: Triangle Universities Nuclear Laboratory, University of North Carolina, Durham, NC 27708-0308, USA

## Abstract

The possible occurrence of highly deformed configurations in the  $^{40}$ Ca di-nuclear system formed in the  $^{28}$ Si +  $^{12}$ C reaction is investigated by analyzing the spectra of emitted light charged particles. Both inclusive and exclusive measurements of the heavy fragments (A  $\geq$  10) and their associated light charged particles (protons and  $\alpha$  particles) have been made at the IReS Strasbourg VIVITRON Tandem facility at bombarding energies of  $E_{lab}(^{28}$ Si) = 112 MeV and 180 MeV by using the ICARE charged particle multidetector array. The energy spectra, velocity distributions, and both in-plane and out-of-plane angular correlations of light charged particles are compared to statistical-model calculations using a consistent set of parameters with spin-dependent level densities. The analysis suggests the onset of large nuclear deformation in  $^{40}$ Ca at high spin.

PACS number(s): 25.70.Gh, 25.70.Jj, 25.70.Mn, 24.60.Dr

#### I. INTRODUCTION

The formation and binary decay of light nuclear systems in the  $A_{CN} \leq 60$  mass region produced by low-energy ( $E_{lab} \leq 7 \text{ MeV/nucleon}$ ) heavy-ion reactions has been extensively studied both from the experimental and the theoretical points of view [1]. In most of the reactions studied the binary breakup of the compound nucleus (CN) is seen as either a fusionfission (FF) [1,2] or a deep-inelastic (DI) orbiting [3] process. The large-angle orbiting yields are found to be particularly strong in the  $^{28}\text{Si} + ^{12}\text{C}$  reaction [4], as illustrated by Fig. 1 which summarizes some of the experimental results that have been collected for this system; i.e., orbiting cross sections [4,5] and total evaporation residue (ER) cross sections [6-12]. Since many of the conjectured features for orbiting yields are similar to those expected for the FF mechanism, it is difficult to fully discount FF as a possible explanation for the large energydamped <sup>28</sup>Si + <sup>12</sup>C yields [3–5]. However, FF calculations [1] significantly underpredict the cross sections measured in the carbon channel by almost a factor of 3, thus suggesting an alternative mechanism (see Fig. 1). FF, DI orbiting, and even molecular-resonance behavior may all be active [13] in the large-angle yields of the  $^{28}$ Si +  $^{12}$ C reaction [14,15]. The backangle elastic scattering of <sup>28</sup>Si ions from <sup>12</sup>C displays structured excitation functions and oscillatory angular distributions in agreement with the relatively weak absorption of this system [16]. Moreover, the resonant gross structure [14] is fragmented into very striking intermediate width resonant structure [15].

Superdeformed (SD) rotational bands have been found in various mass regions (A = 60, 80, 130, 150 and 190) and, very recently, SD bands have also been discovered in the N = Z nuclei  $^{36}$ Ar [17,18] and  $^{40}$ Ca [19]. These new results make the  $A_{CN} \approx 40$  mass region of particular interest since quasimolecular resonances have also been observed in both the  $^{36}$ Ar and  $^{40}$ Ca dinuclear systems [13]. Although there is no experimental evidence to link the SD bands with the higher lying rotational bands formed by known quasimolecular resonances, both phenomena are believed to originate from highly deformed configurations of these systems. Since the detection of light charged particles (LCP) is relatively simple,

the analysis of their spectral shapes is another good tool for exploring nuclear deformation and other properties of hot rotating nuclei at high angular momenta. Experimental evidence for angular-momentum-dependent spectral shapes has already been extensively discussed in the literature [20–34] and, in particular, the  $^{24}$ Mg +  $^{16}$ O reaction [35], which reaches the  $^{40}$ Ca CN, has been studied in detail. Strong deformation effects have also been deduced from angular correlation data for the fusion reaction  $^{28}$ Si( $^{12}$ C,2 $\alpha$ ) $^{32}$ S<sub>g.s.</sub> at E<sub>lab</sub> = 70 MeV [36]. We decided to investigate the  $^{40}$ Ca nucleus produced through the  $^{28}$ Si +  $^{12}$ C reaction at beam energies of E<sub>lab</sub> = 112 MeV and 180 MeV. As can be observed in Fig. 1, model calculations suggest that at the lowest incident energy of the present work the orbiting process is dominant for the C and O channels whereas at E<sub>lab</sub> = 180 MeV a large part of the O and N fully-damped yields may also result from a FF mechanism. In this article we will focus on the LCP's found in coincidence with heavy fragments.

The present paper is organized in the following way. Sec. II describes the experimental procedures and the data analysis. Sec. III presents the inclusive and the exclusive <sup>28</sup>Si + <sup>12</sup>C data (part of the experimental results presented here in detail have already been briefly reported elsewhere [37–41]). The data are analyzed using the Hauser-Feshbach evaporation code CACARIZO [20,21,24] using a consistent set of parameters which has been found to successfully reproduce <sup>24</sup>Mg + <sup>16</sup>O reaction results [35]. The full statistical-model calculations, using Monte Carlo techniques to account for the experimental acceptance when comparing to the experimental exclusive data, are presented in Sec. IV. The strong cluster emission of <sup>8</sup>Be which is observed by the experiment is also discussed in this section. We end with a summary of our conclusion in Sec. V.

### II. EXPERIMENTAL PROCEDURES AND DATA ANALYSIS

The experiments were performed at the VIVITRON Tandem facility of the IReS Strasbourg laboratory using 112 MeV and 180 MeV <sup>28</sup>Si beams which were incident on <sup>12</sup>C targets (160 and 180  $\mu$ g/cm<sup>2</sup> thick, respectively) mounted in the ICARE scattering chamber [44,45].

The effective thicknesses of the  $^{12}$ C targets were accurately determined using Rutherford back scattering (RBS) techniques with  $^{1}$ H and  $^{4}$ He beams provided by the Strasbourg 4 MV Van de Graaff accelerator [39,42,43]. The carbon buildup corrections were found to be less than 2% of the total of C atoms in the targets. Both the heavy fragments (A  $\geq$  10) and their associated LCP's (protons and  $\alpha$  particles) were detected in coincidence using the ICARE charged-particle multidetector array [44,45] which consists of nearly 40 telescopes. Inclusive data have also been collected for heavy fragments and LCP's.

The setup of the measurement at  $E_{lab}(^{28}Si) = 112 \text{ MeV}$  was designed to collect only in-plane coincidences, whereas the setup at  $E_{lab}(^{28}Si) = 180 \text{ MeV}$  allowed both in-plane and out-of-plane angular correlations to be measured (see Table I). The heavy fragments consisting of ER as well as quasi-elastic, deep-inelastic, and fusion-fission fragments were detected in 8 gas-silicon hybrid telescopes (IC), each composed of a 4.8 cm thick ionization chamber, with a thin Mylar entrance window, followed by a 500  $\mu$ m thick Si(SB) detector. The IC's were located at forward angles in two distinct reaction planes (for each plane, the positive and negative angles in Table I are defined in a consistent manner as for the LCP detectors described below). The in-plane detection of coincident LCP's was done using 4 three-element telescopes (TL3) (40  $\mu$ m Si, 300  $\mu$ m Si, and 2 cm CsI(Tl)) placed at forward angles, 16 two-element telescopes (TL2) (40  $\mu$ m Si, 2 cm CsI(Tl)) placed at forward and backward angles and, finally, two other IC telescopes located at the most backward angles (see Table I). The CsI(Tl) scintillators were coupled to photodiode readouts. The IC's were filled with isobutane at a pressure of 30 Torr for the backward angle telescopes and of 60 Torr for the forward angle detectors, thus allowing for the simultaneous measurement of both light and heavy fragments.

For the measurement at  $E_{lab}(^{28}Si) = 180$  MeV, two distinct reaction planes were defined as shown in Table I. One for in-plane correlations and a second one, perpendicular to the LCP detection plane, for out-of-plane correlation measurements. The heavy fragments were detected in 10 IC's located at forward angles for both the in-plane coincidences and outof-plane coincidences. Both the in-plane and out-of-plane coincident LCP's were detected using 3 TL3's placed at forward angles and 24 TL2's placed at forward and backward angles. The IC's were filled with isobutane at a pressure of 60 Torr.

The acceptance of each telescope was defined by thick aluminum collimators. The distances of these telescopes from the target ranged from 10.0 to 30.0 cm, and the solid angles varied from 1.0 msr at the most forward angles to 5.0 msr at the backward angles, according to the expected counting rates.

The energy calibrations of the different telescopes of the ICARE multidetector array were done using radioactive  $^{228}\mathrm{Th}$  and  $^{241}\mathrm{Am}$   $\alpha\text{-particle}$  sources in the 5-9 MeV energy range, a precision pulser, and elastic scatterings of  $112~\mathrm{MeV}$  and  $180~\mathrm{MeV}$   $^{28}\mathrm{Si}$  from  $^{197}\mathrm{Au}$ ,  $^{28}$ Si, and  $^{12}$ C targets in a standard manner. In addition, the  $^{12}$ C( $^{16}$ O, $\alpha$ ) $^{24}$ Mg\* reaction at  $E_{lab} = 53 \text{ MeV}$  [39] was used to provide known energies of  $\alpha$  particles feeding the <sup>24</sup>Mg excited states, thus allowing for calibration of the backward angle detectors. The proton calibration was achieved using scattered protons from  $C_5H_4O_2$  Formwar (polyvinyl formal) targets bombarded in reverse kinematics reactions with both <sup>28</sup>Si and <sup>16</sup>O beams. On an event-by-event basis, corrections were applied for energy loss of heavy fragments (A  $\geq$  10) in the targets and in the entrance window Mylar foils of the IC's and thin Al-Mylar foils of the Si diodes. A correction was also applied for the pulse height defect in the Si detectors. The IC energy thresholds and energy resolution for heavy fragments are better than 1.5 MeV/nucleon and 0.7%, respectively. The total energy resolution of 8.78 MeV  $\alpha$ particles from thorium sources has been found to be better than 2.2% for both the threeelement and two-element light-ion CsI(Tl) telescopes. Absolute cross sections of inclusive measurements could be obtained within 10-12% uncertainties, with 3-5% uncertainties in the target thickness and to 8-10% uncertainties in the electronic deadtime corrections. More details on the experimental setup of ICARE and on the analysis procedures can be found in Refs. [42,43,38–40] and references therein.

#### III. EXPERIMENTAL RESULTS

#### A. Inclusive data

The fragments with Z = 15-17 have inclusive energy spectra that are typical of ER's. The inclusive data of the binary fragments with Z = 5-14 were obtained by integrating their  $1/\sin\theta_{c.m.}$  angular distributions. In particular the results of the cross sections with Z = 6-8 are compared with the previously measured excitation functions [4,5] in Fig. 1. The agreement between both sets of data is satisfactory within the error bars.

The LCP inclusive data can shed some light on the reaction mechanism. Typical inclusive energy spectra of  $\alpha$  particles are shown for the  $^{28}\text{Si}$  +  $^{12}\text{C}$  reaction at  $\text{E}_{lab} = 112$  MeV in Figs. 2-(a) and 2-(b) and at  $\text{E}_{lab} = 180$  MeV in Figs. 2-(c) and 2-(d) at the indicated angles. The solid points (with error bars visible when greater than the size of the points) are the experimental data whereas the solid and dashed lines are statistical model calculations discussed in Sec. IV.B. The  $\alpha$ -particle energy spectra have a Maxwellian shape with an exponential fall-off at high energy which reflects a relatively high effective temperature  $(T_{slope} \approx [8E_{CN}^*/A_{CN}]^{1/2} = 3.67$  MeV for  $E_{lab} = 180$  MeV) of the decaying nucleus. The spectral shape and high-energy slopes are also found to be essentially independent of angle in the c.m. system. These observations suggest a statistical de-excitation process arising from a thermalized source such as the  $^{40}\text{Ca}$  CN and are consistent with a previous study at  $E_{lab} = 150$  MeV [46].

The velocity contour maps of the LCP Galilean-invariant differential cross sections  $(d^2\sigma/d\Omega dE)p^{-1}c^{-1}$  as a function of the LCP velocity are known to provide an overall picture of the reaction pattern. From this pattern the velocity of the emission source can be determined in order to better characterize the nature of the reaction mechanism. Such typical plots [37,39,40,46] (not shown here) can again be understood by assuming a sequential evaporative process and successive emission sources starting with the thermally equilibrated  $^{40}$ Ca\* CN and ending with the final source characterized by a complete freeze-out of the residual nucleus. The Galilean-invariant cross section contours form arcs that are centered at  $V_{c.m.}$  [46], as expected for a complete fusion-evaporation (CF) mechanism followed by

isotropic evaporation.

#### B. Exclusive data

## 1. LCP energy spectra

The exclusive LCP events are also largely consistent with a CF mechanism with the light particles being in coincidence with ER's with Z = 15-17. The data taken with the IC's located at more backward angles (larger than -15°) are not considered in the following analysis since the statistics for fusion-evaporation events are too low. The experimental data of Figs. 3 and 4 are given by the solid points, with error bars visible when greater than the size of the points. At  $E_{lab} = 180$  MeV, the spectral shapes of  $\alpha$  particles in coincidence with P (Z=15) ER's, shown in Fig. 4, are very similar to the inclusive energy spectra of Fig. 2. On the other hand the energy spectra of  $\alpha$  particles in coincidence with S (Z=16) ER's are more complicated as they show other non-evaporative sub-structures (their angular dependence are indicative of a binary decay origin) which are superimposed on the "statistical" Maxwellian shape. These additional non-statistical components will be discussed as arising from a <sup>8</sup>Be cluster emission in Sec. IV.C. At  $E_{lab} = 112$  MeV, shown in Fig. 3, for Z = 15 the high-energy components showing up at the large angles may arise from  $\alpha$ , 3p evaporation cascades.

Fig. 5 presents the corresponding  $^{28}$ Si +  $^{12}$ C exclusive energy spectra of protons emitted in coincidence with individual ER's (Z = 15 and 16) at  $E_{lab} = 180$  MeV. Their spectral shapes are also Maxwellian with the typical exponential fall-off at high energy, characteristic of a statistical CN decay process.

## 2. In-plane angular correlations

The in-plane angular correlations of  $\alpha$  particles and protons in coincidence with ER's produced in the <sup>28</sup>Si + <sup>12</sup>C reaction, are shown in Figs. 6 and 7 at E<sub>lab</sub> = 112 MeV and 180

MeV, respectively. The angular correlations are peaked strongly on the opposite side of the beam direction from the ER detectors which were located at  $\Theta_{lab}^{ER} = -15^{\circ}$  or  $\Theta_{lab}^{ER} = -10^{\circ}$  for the two energies, respectively. The observed peaking of the LCP yields on the opposite side of the beam from the IC is the result of momentum conservation. The angular correlations of both the protons and  $\alpha$  particles show the same behavior for all ER's.

## 3. Out-of-plane angular correlations

Fig. 8 displays the out-of-plane angular correlations of  $\alpha$  particles (circles) and protons (triangles) in coincidence with individual ER's detected at  $\Theta_{lab} = 10^{\circ}$ , produced in the  $^{28}$ Si(180 MeV) +  $^{12}$ C reaction. The angular distributions have a behavior following a typical  $\exp(-asin^2(\theta_{lab}))$  shape [39,47–49], with possibly two components visible for  $\alpha$  particles in coincidence with Z = 14, 15 and 16, plus a broadening of the angular correlations at backward angles. This broadening effect may result from  $\alpha$  particles being able to be emitted at the beginning or at the end of the decay chain, where the angular momentum becomes smaller towards the end of the chain. As the protons cannot remove as much angular momentum as do the  $\alpha$  particles the broadening effect is less significant in the proton angular correlation. The solid lines shown in the figure are the results of statistical-model predictions for CF and equilibrium decay using the Monte Carlo evaporation code CACARIZO [20,21,24], as discussed in the next Section.

#### IV. DISCUSSION

### A. Statistical-model calculations

The evaporation of light particles from a highly excited CN is a well known decay process up to very high excitation energies and spins [50–52]. The interpretation of LCP data requires a careful treatment of the light particle emission properties in the statistical-model description. Most of the available statistical-model computer codes [1,2,50–52] are based

on the Hauser-Feshbach formalism and are able to follow the CN decay by a cascade of evaporated LCP's and neutrons. In particular, a detailed analysis of the exclusive data can be undertaken by the use of Monte Carlo versions [51] of some of these statisticalmodel codes in which the filtering of the events can reproduce the experimental conditions. The statistical-model analysis of the present data has been performed using the Hauser-Feshbach evaporation code CACARIZO [20]. CACARIZO is a Monte Carlo version of the statistical-model code CASCADE [53], which has evolved with many modifications and extensions [20,21,24] from the original code. In this program the effective experimental geometry of the ICARE detectors is properly taken into account. It is assumed that a single CN is created with a well defined excitation energy and angular momentum distribution, and the de-excitation chain is followed step by step and recorded as an event file. The generated events are then analyzed using a subsequent filtering code ANALYSIS [21] in which the locations and the solid angles of all the ICARE telescopes are explicitly specified. This program allows the determination of the different types of events of interest. Such events can be sorted (singles events, coincidence events, etc.) and the corresponding particle spectra and angular distributions can be created.

The CN angular momentum distributions needed as the primary input for the calculations were specified using the critical angular momentum for fusion  $L_{crit}$  and the diffuseness parameter  $\Delta L$ . They were taken from ER cross section data compiled for the <sup>28</sup>Si + <sup>12</sup>C fusion process by Vineyard *et al.* [11], without including fission competition. A fixed value of  $\Delta L = 1\hbar$  (optimized at low energy by a previous statistical-model analysis of this reaction [36]) was assumed for the calculations. It has been checked that the calculated spectra are not sensitive to slight changes in the critical angular momentum or to explicit inclusion of the fission competition. The parameter sets used for the calculations are summarized in Table II.

The other standard ingredients for statistical-model calculations are the formulations of the nuclear level densities and of the barrier transmission probabilities. The transmission coefficients were derived from Optical Model (OM) calculations using potential parameters of light particle induced reactions deduced by Wilmore and Hodgson [54], Perey and Perey [55], and Huizenga [56] for the neutrons, protons and  $\alpha$  particles, respectively. For spin regions where the standard rotating liquid drop model (RLDM) [57] as well as the finite-range liquid drop model (FRLDM) [58] still predict essentially spherical shapes, these sets of transmission coefficients have been found adequate in the considered mass region. However, in recent years it has been observed that when the angular momentum is increased to values for which FRLDM predicts significant deformations, statistical-model calculations using such standard parameters cannot always predict satisfactorily the shape of the evaporated  $\alpha$ particle energy spectra [20–34]. The calculated average energies of the  $\alpha$  particles are found to be much higher than the corresponding experimental results. Several attempts have been made to explain this anomaly either by changing the emission barrier or by using spindependent level densities. Adjusting the emission barriers and corresponding transmission probabilities affects the lower-energy part of the calculated evaporation spectra. On the other hand the high-energy part of the spectra depends crucially on the available phase space obtained from the level densities at high spin. In hot rotating nuclei formed in heavyion reactions, the energy level density at higher angular momentum is spin dependent. The level density,  $\rho(E,J)$ , for a given angular momentum J and energy E is given by the well known Fermi gas expression with equidistant single-particle levels and a constant level density parameter a:

$$\rho(E,J) = \frac{(2J+1)}{12} a^{1/2} \left(\frac{\hbar^2}{2\mathcal{J}_{eff}}\right)^{3/2} \frac{1}{(E-\Delta-T-E_J)^2} \exp(2[a(E-\Delta-T-E_J)]^{1/2}) \quad (1)$$

where T is the "nuclear" temperature and  $\Delta$  is the pairing correction [59]. The quantity  $E_J = \frac{\hbar^2}{2\mathcal{J}_{eff}} J(J+1)$  is the rotational energy, with  $\mathcal{J}_{eff} = \mathcal{J}_0 \times (1 + \delta_1 J^2 + \delta_2 J^4)$  being the effective moment of inertia, where  $\mathcal{J}_0$  at high excitation energy and high angular momentum is considered to be the rigid body moment of inertia and  $\delta_1$  and  $\delta_2$  are the "deformability parameters" [20–22,24,27–34].

The level density parameter is constant and is set equal to  $a = A/8 \text{ MeV}^{-1}$ , a value which is in agreement with previous works [35,60,61]. In principle, the value of a may be affected by

dynamical deformation: rotation induces rearrangement of the single-particle level scheme and the altered nuclear surface area [27] affects the macroscopic energy of the system. The a parameter becomes more important when the nuclear deformation increases [61]. However, in the present work we assume a constant value and rather introduce deformation effects through the deformability parameters. A constant value of a = A/8 is in agreement with various authors [27,35], as well as with theoretical studies by Shlomo and Natowitz [60], by Töke and Swiatecki [61], and with experimental results obtained very recently in the  $A_{CN} = 60$  mass region [62].

No attempt was made to modify the transmission coefficients since it has been shown that the effective barrier heights are fairly insensitive to the nuclear deformation [27]. On the other hand, by changing the deformability parameters  $\delta_1$  and  $\delta_2$  one can simulate the spin-dependent level density [22,24,27,29] associated with a larger nuclear deformation, and thus better reproduce the experimental data.

## B. Deformation effects in <sup>40</sup>Ca

In the present analysis, following the procedure proposed by Huizenga et al. [27], we empirically modify the phase space open to statistical decay by lowering the Yrast line with adjustment of the deformability parameters so as to fit the available experimental data [22,24]. We may also take into account the fact that the deformation should be attenuated during the subsequent emission processes: i.e., there is a readjustment of shape of the nascent final nucleus and a change of collective to intrinsic excitation during the particle-evaporation process. Such an analysis was suggested earlier by Blann and Komoto [64], but with the assumption that the deformation is a frozen degree of freedom through the decay chain. Dynamical effects related to the shape relaxation during the de-excitation process have been incorporated into statistical-model codes [25,28]. For the CACARIZO calculations done here, it is assumed that memory of formation details are lost after each step, with only the conserved quantities such as total energy and spin preserved during the decay sequence.

The CACARIZO calculations have been performed using two sets of input parameters: the first one with standard liquid drop parameters (parameter set A), consistent with the deformation of RLDM [57] and of FRLDM with finite-range corrections of Sierk [58], and the second one with larger values for the deformability parameters [42,43,37,38,41] (parameter set B) which are listed in Table III. In the FRLDM [58] the CN can be considered as spherical or slightly deformed at low bombarding energy, becoming strongly deformed as the spin increases.

The dashed lines in Fig. 2 show the predictions of CACARIZO for  $^{28}$ Si +  $^{12}$ C at both bombarding energies using the parameter **set A** consistent with FRLDM deformation [58]. It can be observed that the average energies of the measured  $\alpha$ -particle inclusive spectra are lower than those predicted by these statistical-model calculations. The solid lines of Fig. 2 show the predictions of CACARIZO using the same increased values of the spin deformation parameters (see parameter **set B** given in Table II) for both energies, and the agreement is considerably improved.

The exclusive energy spectra of the  $\alpha$  particles in coincidence with individual ER's (Z = 15 and Z = 16) are displayed in Figs. 3 and 4 for the two bombarding energies  $E_{lab}$  = 112 MeV and 180 MeV, respectively. It can be observed that the spectra in coincidence with the P residues are well reproduced by using the deformation effects [42,37,38,41]. The solid lines in Figs. 3 and 4 show the predictions of CACARIZO using the parameter set **B** with  $\delta_1 = 2.5 \times 10^{-4}$  and  $\delta_2 = 5.0 \times 10^{-7}$  chosen to reproduce the data consistently at the two bombarding energies. On the other hand, by using the standard liquid drop deformability parameter set **A** with no extra deformation (i.e. with small values of  $\delta_1$  and  $\delta_2$ ), the observed average energies from the exclusive  $\alpha$ -particles spectra are, as found for the inclusive data, lower than those predicted [39] by the statistical model. In this case the CACARIZO parameters are similar to the standard parameters used in a previous study of the 130 MeV  $^{16}O$  + $^{24}$ Mg reaction [35], with the use of the angular momentum dependent level densities.

On inspection of Figs. 3 and 4 a large difference can be noticed when comparing the

calculated and experimental energy spectra associated with S residues and those associated with P ER's [38]. The latter are reasonably well reproduced by the CACARIZO calculations, whereas the model does not predict the shape of the spectra obtained in coincidence with S residues at backward angles ( $\theta_{\alpha} \geq 40^{\circ}$  at  $E_{lab} = 112$  MeV and  $\theta_{\alpha} \geq 70^{\circ}$  at  $E_{lab} = 180$  MeV). An additional, non-statistical,  $\alpha$ -particle component is suggested in Section IV.C to arise from a <sup>8</sup>Be emission process. This is consistent with the discrepancies also observed at backward angles in the in-plane angular correlations of Fig. 6. For both  $\alpha$  particles and protons the calculations significantly underpredict the yields at the negative angles at  $E_{lab} = 112$  MeV. However the agreement is more satisfactory for protons at  $E_{lab} = 180$  MeV as shown in Fig. 7.

As shown in Fig. 5 CACARIZO calculations are also able to reproduce the shape of exclusive proton spectra for the  $^{28}$ Si(180 MeV) +  $^{12}$ C reaction. Compared to the  $\alpha$  particles, it may be mentioned that the energy spectra of the protons do not shift as significantly as the spin-dependent parametrization of the moment of inertia is introduced. The statistical-model results using the two different parameter sets reproduce equally well the experimental velocity spectra and angular correlations. The statistical-model calculations displayed for protons in Fig. 5 have been performed with parameter set **B** (solid lines) including the deformation effects (calculated curves with parameter set **A** are indistinguishable from the solid lines).

In order to better determine the magnitude of the influence of deformation effects in the CN and the residual nuclei which are suggested by our choice of statistical-model approach, we have proposed a very simple procedure [43,47–49]. The effective moment of inertia is expressed as  $\mathcal{J}_{eff} = \frac{2}{5} \mathrm{MR}^2 = \frac{1}{5} \mathrm{M}(b^2 + a^2)$  with the volume conservation condition: V =  $\frac{4}{3}\pi abc$ , where b and a are the major and minor axis, and c is the rotational axis of the CN. In the case of an oblate shape a = b and  $\mathcal{J}_{eff} = \frac{2}{5} \mathrm{Ma}^2$  and  $V = \frac{4}{3}\pi a^2 c$ . The axis ratio is equal to  $\delta = a/c = (1+\delta_1 \mathrm{J}^2 + \delta_2 \mathrm{J}^4)^{3/2}$ . In the case of a prolate shape a = c and  $\mathcal{J}_0 = \frac{1}{5} \mathrm{M}(b^2 + a^2)$  and  $V = \frac{4}{3}\pi a^2 b$ . We obtain the equation:  $1+(3-\gamma)x+3x^2+x^3=0$  with  $x=\left(\frac{b}{a}\right)^2 = \delta^2$  and  $\gamma = 8(1+\delta_1 \mathrm{J}^2 + \delta_2 \mathrm{J}^4)^3$ . The quadrupole deformation parameter  $\beta$  is equal to  $\beta = \frac{1}{3} \mathrm{M}(b^2 + a^2)$  and  $\beta = \frac{1}{3} \mathrm{M}(b^2 + a$ 

$$\frac{1}{\sqrt{5\pi}}(\frac{4}{3}\delta + \frac{2}{3}\delta^2 + \frac{2}{3}\delta^3 + \frac{11}{18}\delta^4).$$

The effects of the Yrast line lowering (increase of the level density) due to the nuclear deformation and the variation of the deformation parameter  $\beta$  can be quantitatively discussed using the values in Table III for several reactions. The values of the minor to major axis ratio b/a and of the deformation parameter  $\beta$  have been extracted (with 10% error bars) from the fitted deformability parameters by assuming a symmetric prolate shape with sharp surfaces [27]. The assumption of oblate shapes yields similar results within 5%. It is interesting to note that the deformation found necessary to reproduce the <sup>28</sup>Si + <sup>12</sup>C reaction results is smaller than the deformation introduced by the deformability parameter used by Kildir *et al.* [46], who also change the transmission coefficients.

The solid lines shown in Figures 6 and 7 are the results of CACARIZO calculations for the exclusive measurements. It can be observed in Fig. 6 that for  $E_{lab} = 112$  MeV the experimental angular correlations are well reproduced by the evaporation calculations for the data at the opposite side from the ER detector, and this is true for correlations with both S and P ER's. However the calculations fail to predict the experimental data at the same side as the ER detector. The question of these large yields measured at negative angles remains open [43]. Similarly the CACARIZO calculations reproduce in Fig. 7 the in-plane angular correlations of  $\alpha$  particles (circles) and protons in coincidence with all ER's, at  $E_{lab} = 180$  MeV, for the data on the opposite side from the ER detector. They are also able to describe the in-plane angular correlations of protons in coincidence with individual Z = 14 and Z = 15 on both sides of the beam. However, the excess of yields observed at backward angles  $(\Theta_{lab} = +50^{\circ} \text{ to } +90^{\circ})$  for  $\alpha$  particles in coincidence with S may indicate the occurrence of a non-evaporative process, possibly of a binary nature. The excess of yields is even stronger for  $\alpha$  particles in coincidence with Si. Here the hypothesis of a non-evaporative component arising from the <sup>12</sup>C breakup may be advanced.

The solid lines shown in Fig. 8 for the out-of-plane angular correlations are the results of CACARIZO statistical-model predictions. Once again it can be observed that the

statistical-model calculations are able to reproduce the proton coincidences well, but they fail to describe the  $\alpha$ -Cl coincidences and the large yields found in coincidence with P and Si ER's in the most forward direction. The poor reproduction of the  $\alpha$ -particle experimental anisotropy factor is not well understood. The angular momentum dependence has been tested by performing calculations with two different angular-momentum windows:  $10\text{-}20\hbar$  and  $20\text{-}30\hbar$ . Whereas for protons the anisotropy is almost constant with the L-window, for the  $\alpha$  particles the anisotropy is strongly depending of the chosen L-window. Nevertheless the flat behavior shown around  $0^{\circ}$  is present for the two particle species. The observed discrepancy suggests that the assumed angular distribution of the LP, which is handled semi-classically, may not be adequate to describe the out-of-plane data.

Overall, we conclude that the evaporated  $\alpha$  particles from  $^{40}$ Ca CN emission reflect significant deformation effects. The deduced deformation is comparable to that found previously in the analysis of  ${}^{28}{\rm Si}({}^{12}{\rm C},2\alpha){}^{32}{\rm S}_{g.s.}$  angular correlation data [36]. The extent to which these effects can be reasonably well quantified is dependent on the experimental coverage and, in particular, on the power of the coincidence trigger. It is of particular interest to note that the value of  $\beta \approx 0.5$  found for the quadrupole deformation parameter of  $^{28}\text{Si} + ^{12}\text{C}$  (see Table III) might be connected with the recent observation of SD bands in the doubly-magic <sup>40</sup>Ca nucleus by standard  $\gamma$ -ray spectroscopy methods [19]. Correlating large prolate deformations in the hot CN with the presence of SD bands in <sup>40</sup>Ca is obviously not straightforward, since the deformation deduced from the LCP data averages over CN configurations, while the SD bands are based on one of these configurations. We made the same discussion with the possible comparison between LCP results for the  $^{28}{\rm Si}$  +  $^{28}{\rm Si}$  reaction [43] and  $\gamma$ -ray data displaying very deformed bands in the doubly magic <sup>56</sup>Ni nucleus [65]. It is interesting to add that the macroscopic deformation energy of <sup>40</sup>Ca recently calculated within a Generalized Liquid Drop Model [66] with shell effects (using the Strutinsky method) generates a second highly deformed minimum where SD and highly deformed states may survive.

## C. Non-statistical <sup>8</sup>Be cluster emission

It has been shown from the analysis of Figs. 3 and 4 with CACARIZO that additional non-statistical components appear to be significant at both  $E_{lab}=112~\mathrm{MeV}$  and 180 MeV bombarding energies. However no evidence was found for additional processes at the lower bombarding energies of  $E_{lab} = 70 \text{ MeV} [36]$  and 87 MeV [67]. To better understand the origin of these components,  $\alpha$  particle energies are plotted in Fig. 9 against the energies of the S residues detected at  $\Theta_S = -10^\circ$  for the  $^{28}{\rm Si}(180~{\rm MeV})$  +  $^{12}{\rm C}$  reaction for a number of  $\alpha$ -particle emission angles. With increasing  $\alpha$ -particle angles an increase of the energy of S residues and a decrease of the  $\alpha$  energy is observed which is consistent with kinematics. At  $\Theta_{\alpha} = +40^{\circ}$ ,  $+45^{\circ}$ , and  $+50^{\circ}$  the bulk of events in Fig. 9 are of a statistical origin, and consistent with CACARIZO calculations, as demonstrated in Fig. 10-(b) (for  $\Theta_{\alpha} = +40^{\circ}$ ). Another statistical-model code PACE 2 [68] gives similar predictions. The calculations suggest that these  $\alpha$  particles result from a cascade of a single  $\alpha$ , two protons, and x neutrons rather than a 2- $\alpha$ , xn evaporation process. For larger angles, the two branches, corresponding to the contours labeled 1 and 2, although lying outside the "statistical evaporation region", still correspond to an evaporation process as shown by the CACARIZO calculations displayed in Fig. 10-(b) for  $\Theta_{\alpha} = +40^{\circ}$  and in Fig. 10-(d) for  $\Theta_{\alpha} = +70^{\circ}$ . These two branches 1 and 2 correspond to a  $2-\alpha$  fusion-evaporation channel with both the  $\alpha$  particles emitted respectively at backward and forward angles in the center of mass. However, at more backward angles other additional contributions, corresponding to the strong peak in the contour labeled 2 and in the contours labeled 3 and 4, appear with increasing significance, as shown, for instance in Fig. 10-(c) for  $\Theta_{\alpha}=+70^{\circ}$ . The corresponding "folding angles" are compatible with the two-body kinematics required for the  $^{32}S + ^{8}Be$  binary exit-channel. In contrast, the energy correlations for the  $\alpha$  particles in coincidence with Cl and P residues (not shown) do not exhibit similar two-body branches, the "statistical evaporation region" is consistent with the CACARIZO predictions, for all the measured angles.

Although in principle the identification of the <sup>8</sup>Be cluster requires the coincident detec-

tion and mass identification of both decaying  $\alpha$  particles [69], a kinematic reconstruction assuming a two-body <sup>32</sup>S + <sup>8</sup>Be\* process is instructive. Assuming the three-body kinematics of a  $\alpha + \alpha + 3^2$ S final state, it is possible to reconstruct the momentum of the "missing"  $\alpha$ -particle and, hence, to deduce the excitation energy of the intermediate <sup>8</sup>Be fragment. In Figs. 11 the deduced excitation energy spectra in this channel are presented for the contributions labeled 2, 3, and 4 in Fig. 10-(c) at the indicated  $\Theta_{\alpha}$  angles. From  $\Theta_{\alpha} = 70^{\circ}$ to  $\Theta_{\alpha} = 85^{\circ}$  the strongest peak appears with a very narrow width. This large component, which corresponds to the contribution of the contour 4 visible in Fig. 10-(c), is centered at the energy of the ground state of  ${}^8\mathrm{Be}$  (the relative energy of the two  $\alpha$  particles of the  ${}^8\mathrm{Be}$ breaking up in flight is 92 keV) and displayed as the squared part of Fig. 11-(a). From  $\Theta_{\alpha}$  = 55° to  $\Theta_{\alpha}=95$ ° the main bulk of the yields from contours 2 and 3 is centered at around E\* = 3.1 MeV with an experimental width of approximately 1.5 MeV, which values correspond well to the known energy (E\* = 3.04 MeV) and width ( $\Gamma = 1500 \text{ keV}$ ) of the first 2<sup>+</sup> excited level of  ${}^8\mathrm{Be}$  [70]. The short-lived  ${}^8\mathrm{Be}$  4<sup>+</sup> excited level at  $\mathrm{E}^* = 11.4~\mathrm{MeV}$  [71] is not clearly observed due to its very broad width ( $\Gamma = 3.7 \text{ MeV}$ ) and the significant  $\alpha$ -statistical background arising from the contribution of the contour 2. For the same reasons it is hazardous to assign the bumps around 15 MeV to the known  $2^+$  doublet [70] at  $E^* = 16.6$  and 16.9MeV.

Figs. 11-(b) and 11-(c) display the reconstructed excitation energy spectra of the S binary fragments measured at  $\Theta_S = -10^{\circ}$  in coincidence with  $\alpha$  particles detected at the indicated  $\Theta_{\alpha}$  angles by gating either on the ground state (g.s.) contour 4 (upper panel) or the  $2^+$  state contours 2 and 3 (lower panel). We have performed fusion-fission calculations (not shown), using the Extended Hauser-Feshbach Method [2]. They fail to reproduce both the excitation energies of the  $^{32}$ S fragments, and the yields from the contributions 2, 3 and 4 [37]. These contributions might result from a faster binary process governed by the  $\alpha$ -transfer reaction mechanism  $^{28}$ Si +  $^{12}$ C  $\rightarrow$   $^{32}$ S\* +  $^{8}$ Be, as proposed by Morgenstern *et al.* [72]. This conclusion is in agreement with previous inclusive results published in Ref. [12]. In the cluster-transfer picture [72] the reaction is characterized by a "Q-value" window centered at the so-called

"Q-optimum", which value can be estimated semi-classically by  $Q_{opt} = (Z_3Z_4/Z_1Z_2-1)E_i^{c.m.}$ , where the indices 1,2 and 3,4 indicate the entrance (i) and exit channel, respectively. The corresponding excitation energy  $E^* = Q_{gg}$  -  $Q_{opt}$ , where  $Q_{gg}$  is the ground-state Q-value of the reaction. In this case the expected excitation energy in the <sup>32</sup>S nuclei is equal to 12.9 MeV. Fig. 11 represents the calculated excitation energy of <sup>32</sup>S in coincidence with the g.s. (b) for individual angles and by adding individuals angles (lower spectrum labelled Total), and with the first  $2^+$  (E $_x=3.04$  MeV) excited state (c) of  $^8$ Be, respectively. The strong shifts of the energy distributions can be explained by the bias effects induced by the kinematic coincidence acceptances. The dashed lines correspond to  $E^* = 12.9$  MeV, the energy expected for  $\alpha$ -transfer reaction mechanisms. In both cases the excitation energies (total spectra for the coincidence with the g.s.) of <sup>32</sup>S are consistent with these values. In the same way we can also have a  $^8{\rm Be\text{-}transfer}$  reaction mechanism [12]  $^{28}{\rm Si}$  +  $^{12}{\rm C}$   $\rightarrow$   $^{36}{\rm Ar}^*$  +  $\alpha$ . In this case the  $^{36}{\rm Ar}^*$  ejectile has sufficient excitation energy to emit either one proton or one  $\alpha$  particle. This type of "transferlike" reaction can explain the disagreement observed in Fig. 6 between data and CACARIZO calculation for the in-plane angular correlation between  $\alpha$  particles and Cl residues.

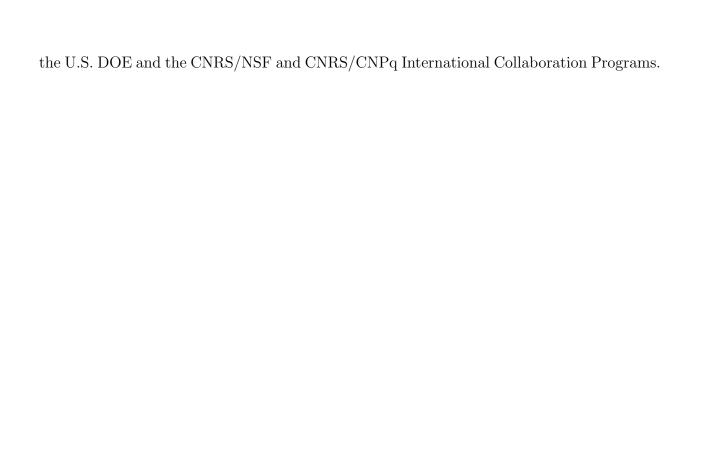
### V. CONCLUSIONS

The possible occurrence of highly deformed configurations in the  $^{40}$ Ca dinuclear system has been investigated by using the ICARE charged-particle multidetector array at the VIVITRON Tandem facility of the IReS Strasbourg. The properties of the emitted LCP's in the  $^{28}$ Si +  $^{12}$ C reaction have been analyzed at two bombarding energies  $E_{lab} = 112$  MeV and 180 MeV, and compared with a statistical model that was adopted to calculate evaporation spectra and angular distributions for deformed nuclei. A Monte Carlo technique has been employed in the framework of the well documented Hauser-Feshbach code CACARIZO. The measured observables such as velocity distributions, energy spectra, in-plane and out-of-plane angular correlations are all reasonably well described by the Monte Carlo calculations

which include spin-dependent level densities. The magnitude of the adjustments in the Yrast line suggests deformations at high spins in the  $^{40}$ Ca dinuclear system that are far in excess of those predicted by the FRLDM. The deduced deformations are comparable to recent  $\gamma$ -ray spectroscopy data for the  $^{40}$ Ca nucleus at much lower spins [19]. The suggested  $^{40}$ Ca shapes are consistent with predictions of the Generalized Liquid Drop Model [66] which predicts a second highly deformed minimum in this system resulting from shell effects where SD and highly deformed states may survive. A component is found in the  $\alpha$ -particle energy spectra measured in coincidence with S residues that is attributed to the decay of unbound  $^{8}$ Be nuclei, although this study does not clearly establish the mechanism resulting in these yields. In general, to fully explore the influence of nuclear deformation on the reaction mechanisms and underlying nuclear structure in the mass  $A \approx 40$  region will require sophisticated particle- $\gamma$  experiments (see Refs. [73–76] for instance) using EUROBALL IV and/or GAMMASPHERE. These studies are necessary to better understand how the large nuclear deformations that are apparent in the fusion studies are related to the superdeformed bands discovered and/or predicted in this mass region [17–19].

### ACKNOWLEDGMENTS

This paper is based upon the Ph.D. thesis of M. Rousseau, Université Louis Pasteur, Strasbourg, 2000. The authors would like to thank the staff of the VIVITRON for providing us with good stable beams, and J. Devin and C. Fuchs for their excellent support in carrying out these experiments. Particular appreciation to M.A. Saettel for preparing the targets, and to J.P. Stockert and A. Pape for assistance during their RBS measurements. We also whish to thank N. Rowley and W. Catford for useful discussions and for a careful reading of the manuscript. One of us (M.R.) would like to acknowledge the Conseil Régional d'Alsace for the financial support of his Ph.D. thesis work. Parts of this work has also been done in collaboration with C.E. during his summer stay at the IReS with a JANUS Grant of IN2P3. This work was sponsored by the French CNRS/IN2P3. Additional support was supplied by



## REFERENCES

- [1] S. J. Sanders, A. Szanto de Toledo, and C. Beck, Phys. Rep. **311**, 487 (1999).
- [2] T. Matsuse, C. Beck, R. Nouicer, and D. Mahboub, Phys. Rev. C 55, 1380 (1997).
- [3] B. Shivakumar, S. Ayik, B. A. Harmon, and D. Shapira, Phys. Rev. C 35, 1730 (1987).
- [4] D. Shapira, R. Novotny, Y. C. Chan, K. A. Erb, J. L. C. Ford jr., J. C. Peng, and J. D. Moses, Phys. Lett. 114B, 111(1982); D. Shapira, D. Schull, J. L. C. Ford, Jr., B. Shivakumar, R. L. Parks, R. A. Cecil, and S. T. Thornton, Phys. Rev. Lett. 53, 1634 (1984).
- [5] D. Shapira, D. Schull, J. L. C. Ford, Jr., B. Shivakumar, R. L. Parks, R. A. Cecil and S. T. Thornton, Phys. Rev. Lett. 53, 1634 (1984).
- [6] S. Gary and C. Volant, Phys. Rev. C 25, 1877 (1982).
- [7] K. T. Lesko, D. -K. Lock, A. Lazzarini, R. Vandenbosch, V. Metag, and H. Doubre, Phys. Rev. C 25, 872 (1982).
- [8] Y. Nagashima, S. M. Lee, M. Sato, J. Schimizu, T. Nakagawa, Y. Fukuchi, K. Furuno, M. Yamanouchi, and T.Mikumo, Phys. Rev. C 26, 2661 (1982).
- [9] B. A. Harmon, S. T. Thornton, D. Shapira, J. Gomez del Campo, and M. Beckerman, Phys. Rev. C 34, 552 (1986).
- [10] B. A. Harmon, D. Shapira, P. H. Stelson, B. L. Burks, K. A. Erb, B. Shivakumar, K. Teh, and S. T. Thornton, Phys. Rev. C 38, 572 (1988).
- [11] M. F. Vineyard et al., Phys. Rev. C 47, 2374 (1993).
- [12] N. Arena, Seb. Cavallaro, S. Femino, P. Figuera, S. Pirrone, G. Politi, F. Porto, S. Romano, and S. Sambataro, Phys. Rev. C 50, 880 (1994).
- [13] D. Pocanic and N. Cindro, Nucl. Phys. A433, 531 (1985); and references therein.

- [14] R. Ost, M. R. Clover, R. M. DeVries, B. R. Fulton, H. E. Gove, and N. J. Rust, Phys. Rev. C 19, 740 (1979).
- [15] J. Barrette, M. J. LeVine, P. Braun-Munzinger, G. M. Berkowitz, M. Gai, J. W. Harris, C. M. Jachcinski, and C. D. Uhlhorn, Phys. Rev. C 20,1759 (1979).
- [16] C. Beck, Y. Abe, N. Aissaoui, B. Djerroud and F. Haas, Phys. Rev. C49, 2618(1994); and references therein.
- [17] C. E. Svensson et al., Phys. Rev. Lett. 85, 2693 (2000); Nucl. Phys. A682, 1 (2001).
- [18] C. E. Svensson *et al.*, Phys. Rev. C **63**,061301(R) (2001).
- [19] E. Ideguchi et al., Phys. Rev. Lett. 87,222501 (2001).
- [20] R. K. Choudhury, P. L. Gonthier, K. Hagel, M. N. Namboodiri, J. B. Natowitz, L. Adler, S. Simon, S. Kniffen et G. Bergowitz, Phys. Lett. B143, 74 (1984).
- [21] Z. Majka, M. E. Brandan, D. Fabris, K. Hagel, A. Menchaca-Rocha, J. B. Natowitz, G. Nebbia, G. Prete, B. Sterling et G. Viesti, Phys. Rev. C 35, 2125 (1987).
- [22] I. M. Govil, J. R. Huizenga, W. U. Schröder, and J. Töke, Phys. Lett. B 197, 515 (1987).
- [23] B. Fornal, G. Prete, G. Nebbia, F. Trotti, G. Viesti, D. Fabris, K. Hagel, and J. B. Natowitz, Phys. Rev. C 37, 2624 (1988).
- [24] G. Viesti, B. Fornal, D. Fabris, K. Hagel, J. B. Natowitz, G. Nebbia, G. Prete, and F. Trotti, Phys. Rev. C 38, 2640 (1988).
- [25] B. Fornal, G. Viesti, G. Nebbia, and J. B. Natowitz, Phys. Rev. C 40, 664 (1989).
- [26] G. La Rana et al., Phys. Rev. C 37, 1920 (1988); ibidem C 40, 2425 (1989).
- [27] J. R. Huizenga, A. N. Behkami, I. M. Govil, W. U. Schröder, and J. Töke, Phys. Rev. C 40, 668 (1989).

- [28] B. Fornal, F. Gramegna, G. Prete, R. Burch, G. D'Erasmo, E. M. Fiore, L. Fiore, A. Pantaleo, V. Paticchio, G. Viesti, P. Blasi, N. Gelli, F. Lucarelli, M. Anghinolfi, P. Corvisiero, M. Taiuti, A. Zucchiatti, P. F. Bortignon, J. Ruiz, G. Nebbia, M. Gonin, and J. B. Natowitz,
  Phys. Lett. B 255, 325 (1991).
- [29] D. K. Agnihotri, A. Kumar, K. C. Jain, K. P. Singh, G. Singh, D. Kabiraj, D. K. Avasthi, and I. M. Govil, Phys. Lett. B 307, 283 (1993).
- [30] I. M. Govil, R. Singh, A. Kumar, J. Kaur, A. K. Sinha, N. Madhavan, D. O. Kataria, P. Sugathan, S. K. Kataria, K. Kumar, Bency John, and G. V. Ravi Prasad, Phys. Rev. C 57, 1269 (1998).
- [31] D. Bandyopadhyay, S. K. Basu, C. Bhattacharya, S. Bhattacharya, K. Krishan, A. Chatterjee, S Kailas, A. Navin, and A. Shrivastava, Phys. Rev. C 59, 1179 (1999).
- [32] I. M. Govil, R. Singh, Ajay Kumar, G. Singh, S. K. Kataria, and S. K. Datta, Phys. Rev. C 62, 064606 (2000).
- [33] I. M. Govil, R. Singh, A. Kumar, S. K. Datta, and S. K. Kataria, Nucl. Phys. A674, 377 (2000).
- [34] D. Bandyopadhyay, C. Bhattacharya, K. Krishan, S. Bhattacharya, S.K. Basu, A. Chatterjee, S Kailas, A. Shrivastava, and K. Mahata, Phys. Rev. C **64**, 064613 (2001).
- [35] B. Fornal *et al.*, Phys. Rev. C **44**, 2588 (1991).
- [36] N. Alamanos, C. Levi, C. Le Metayer, W. Mittig, and L. Papineau, Phys. Lett. 127B, 23 (1983).
- [37] M. Rousseau *et al.*, in Proceedings of the 7<sup>th</sup> International Conference on Clustering Aspects of Nuclear Structure and Dynamics, eds. M. Korolija, Z. Basrak and R. Caplar (World Scientific Publishing Co., Singapore, 2000), p.189.

- [38] C. Beck et al., in Proceedings of the 9<sup>th</sup> International Conference on Nuclear Reactions, Varenna, Italy, 2000, edited by E. Gadioli [Ricerca Scientifica ed Educatione Permanente, Suppl. 115, (2000) p. 407].
- [39] M. Rousseau, Ph.D. thesis, Strasbourg University, Report **IReS 01-02** (2001) (unpublished).
- [40] M. Rousseau et al., in Proceedings of the XXXIX International Winter Meeting on Nuclear Physics, Bormio, Italy, 2001, edited by I. Iori [Ricerca Scientifica ed Educatione Permanente, Suppl. 117, (2001) p. 370.].
- [41] C. Bhattacharya et al., in Proceedings of the Workshop on Physics with Multidetector Arrays, Saha Institute of Nuclear Physics, Calcutta, India, 2000, Pramana Indian Journal of Physics Vol. 57No. 1, (2001) p. 203.
- [42] C. Bhattacharya et al., Nucl. Phys. A654, 841c (1999).
- [43] C. Bhattacharya, M. Rousseau, C. Beck, V. Rauch, R.M. Freeman, D. Mahboub, R. Nouicer, P. Papka, O. Stezowski, A. Hachem, E. Martin, A.K. Dummer, S.J. Sanders, and A. Szanto De Toledo, Phys. Rev. C 65, 014611 (2002).
- [44] G. Bélier, Ph.D. thesis, Strasbourg University, Report **CRN-94-34** (1994) (unpublished).
- [45] T. Bellot, Ph.D. thesis, Strasbourg University, Report IReS-97-35 (1997) (unpublished).
- [46] M. Kildir et al., Phys. Rev. C 51, 1873 (1995).
- [47] C. Beck et al., Ricerca Scientifica ed Educazione Permanente Supp. 101, 127 (1995).
- [48] D. Mahboub, Ph.D. thesis, Strasbourg University, Report CRN-96-36 (1996) (unpublished).
- [49] D. Mahboub et al., to be published

- [50] R. G. Stokstad, *Treatise on Heavy Ion Science* vol.3, ed. D. A. Bromley (New York; Plenum) (1985).
- [51] A. J. Cole, *Statistical Models for Nuclear Decay*,ed. R. R. Betts and W. Greiner (IOP Publishing, Bristol and Philadelpia) (2000).
- [52] R. J. Charity, Phys. Rev. C **61**, 054614 (2000).
- [53] F. Pühlhofer, Nucl. Phys. **A280**, 267 (1977).
- [54] D. Wilmore and P. E. Hodgson, Nucl. Phys. **55**, 673 (1964).
- [55] F. G. Perey, Phys. Rev. 131, 745 (1963); C. M. Perey and F. G. Perey, Nucl. Data Tables 17, 1 (1976).
- [56] J. R. Huizenga, Nucl. Phys. 29, 29 (1961).
- [57] S. Cohen, F. Plasil, and W. J. Swiatecki, Ann. Phys. (N.Y.) 82, 557 (1974).
- [58] A. J. Sierk, Phys. Rev. C **33**, 2039 (1986).
- [59] W. Dilg, W. Schantl, H. Vonach, and M. Uhl, Nucl. Phys. **A217**, 269 (1973).
- [60] S. Shlomo and J. B. Natowitz, Phys. Rev. C 44, 2878 (1991).
- [61] J. Töke and W. J. Swiatecki, Nucl. Phys. **A372**, 141 (1981).
- [62] P. Jänker, H. Leitz, K. E. G. Löbner, M. Morales, and H. G. Thies, Eur. Phys. J. A 4, 147 (1999).
- [63] W.D. Myers and W.J. Swiatecki, Nucl. Phys. 81, 1 (1966).
- [64] M. Blann and T. T. Komoto, Phys. Rev. C 24, 486 (1981).
- [65] D. Rudolph et al., Phys. Rev. Lett. 82, 3763 (1999); Eur. Phys. J. A 4, 115 (1999).
- [66] G. Royer, C. Bonilla, and R. A. Gherghescu, Phys. Rev. C 65, 067304 (2002).
- [67] R. Ost, A.J. Cole, M.R. Clover, B.R. Fulton and B.Sikora, Nucl. Phys. A342, 185

(1980).

- [68] A. Gavron, Phys. Rev. C 21, 230 (1980).
- [69] E. W. MacDonald, A. C. Shotter, D. Branford, J. Rahighi, T. Davinson, N. J. Davis, Y. El-Mohri, and J. Yorkston, Nucl. Instrum. Methods Phys. Res. A317, 498 (1992).
- [70] F. Ajzenberg-Selove, Nucl. Phys. **A490**, 1 (1988).
- [71] N. Arena, Seb. Cavallaro, P. D'Agostino, G. Fazio, G. Giardina, O. Yu Goryunov, V. V. Ostahko, R. Palamara, and A. A. Shvedov, J. Phys. G: Nucl. Part. Phys. 21, 1403 (1995).
- [72] H. Morgenstern, W. Bohne, W. Galster, and K. Grabisch, Z. Phys. A **324**, 443 (1986).
- [73] R. Nouicer, C. Beck, R. M. Freeman, F. Haas, N. Aissaoui, T. Bellot, G. de France, D. Disdier, G. Duchène, A. Elanique, A. Hachem, F. Hoellinger, D. Mahboub, V. Rauch, S. J. Sanders, A. Dummer, F. W. Prosser, A. Szanto de Toledo, Sl. Cavallaro, E. Uegaki, and Y. Abe, Phys. Rev. C 60, 41303 (1999).
- [74] C. Beck, R. Nouicer, D. Disdier, D. Duchène, G. de France, R. M. Freeman, F. Haas, A. Hachem, D. Mahboub, V. Rauch, M. Rousseau, S. J. Sanders, and A. Szanto de Toledo, Phys. Rev. C 63, 014607 (2001).
- [75] S. Thummerer et al., Phys. Scr. **T88**, 114 (2000).
- [76] S. Thummerer, W. von Oertzen, B. Gebauer, D. R. Napoli, S. M. Lenzi, A. Gadea, C. Beck, and M. Rousseau, J. Phys. G: Nucl. Part. Phys. 27, 1405 (2001).

TABLES

ICARE SETUP											
$^{28}\text{Si}(112 \text{ MeV}) + ^{12}\text{C}$			$^{28}\mathrm{Si}(180\ \mathrm{MeV})+^{12}\mathrm{C}$								
Type of detector	$ heta(^{\circ})$	φ(°)	Type of detector	$\theta(^{\circ})$	φ(°)						
IC	±15	0	IC	±10	0						
	-20	+20		+10	90						
	$\pm 25$	0		$\pm 15$	0						
	-30	+20		$\pm 20$	0						
	-35	0		+20	90						
	-40	+20		$\pm 25$	0						
	+130	0		-	-						
	-150	0		-	-						
TL3	+15	+20	TL3	±30	0						
	+25	+20		+35	0						
	+35	+20		-	-						
	+45	+20		-	-						
TL2	16 te	lescopes each 5° from	$\mathrm{TL}2$	24 telescopes each 5° from							
	$\theta = 40$	$0^{\circ}$ to $115^{\circ}$ and $\phi=0^{\circ}$		$\theta{=}40^{\circ}$ to 95° and $\phi{=}0^{\circ}$							

TABLE I. Experimental setup of ICARE chosen for the  $^{28}Si + ^{12}C$  reaction at  $E_{lab} = 112$  MeV and 180 MeV.

## Angular-momentum distribution in CN

Critical angular momenta  $L_{cr}=21~(\mathrm{E}_{lab}=112~\mathrm{MeV})$  and  $27\hbar~(\mathrm{E}_{lab}=180~\mathrm{MeV}).$ Diffuseness parameter  $\Delta L = 1.0\hbar$ .

## OM potentials of the emitted LCP and neutrons

- (1) Transmission coefficients as defined in the text
- (2) Multiply factor of the OM radius: RFACT = 1

# Level-density parameters at low excitation: $(E^* \le 10 \text{ MeV})$

- (1) Fermi-gas level-density formula with empirical level-density parameters from Dilg et al. [59]
- (2) Effective moment of inertia  $\Im = IFACT \Im_{rigid}$  with IFACT = 1.

# Level-density parameters at high excitation: $(E^* \ge 20 \ \mathrm{MeV})$

- (1) Fermi-gas level-density formula with parameters from RLDM (Myers and Swiatecki [63])
- (2) Level-density parameter:  $a = A/8 \text{ MeV}^{-1}$

### Yrast line

- Parameter set A: FRLDM (Sierk [58])
- Parameter set **B**:  $\Im = \Im_{sphere}(1 + \delta_1 J^2 + \delta_2 J^4)$  with  $\delta_1 = 2.5 \ 10^{-4}$  et  $\delta_2 = 5.0 \ 10^{-7}$   $\gamma$ -ray width (in Weisskopf units)

- (1) E1: B(E1) = 0.001
- (2) M1: B(M1) = 0.01
- (3) E2: B(E2) = 5.0

TABLE II. Parameter sets used in the CACARIZO calculations for the  $^{28}Si + ^{12}C$  reaction at  $E_{lab} = 112 \text{ and } 180 \text{ MeV}.$ 

Reaction	C.N.	$L_{cr}$ $(\hbar)$	$\delta_1$	$\delta_2$	b/a	β	Reference
$^{28}{\rm Si} + ^{12}{\rm C}$	$^{40}\mathrm{Ca}$	21	$2.5 \cdot 10^{-4}$	$5.0 \cdot 10^{-7}$	1.3	0.47	This work
$^{28}{\rm Si} + ^{12}{\rm C}$	$^{40}\mathrm{Ca}$	26	$6.5 \cdot 10^{-4}$	$3.3 \cdot 10^{-7}$	2.0	0.53	[46]
$^{28}{\rm Si} + ^{12}{\rm C}$	$^{40}\mathrm{Ca}$	27	$2.5 \cdot 10^{-4}$	$5.0 \cdot 10^{-7}$	1.8	0.51	This work
$^{28}{\rm Si} + ^{27}{\rm Al}$	$^{55}\mathrm{Co}$	42	$1.8 \cdot 10^{-4}$	$1.8 \cdot 10^{-7}$	1.3	0.46	[29]
$^{28}{\rm Si} + ^{28}{\rm Si}$	$^{56}\mathrm{Ni}$	34	$1.2 \cdot 10^{-4}$	$1.1 \cdot 10^{-7}$	1.6	0.49	[43]
$^{28}{\rm Si} + ^{28}{\rm Si}$	$^{56}\mathrm{Ni}$	37	$1.2 \cdot 10^{-4}$	$1.1 \cdot 10^{-7}$	1.7	0.50	[39]
$^{30}Si + ^{30}Si$	$^{60}\mathrm{Ni}$	34	$1.2 \cdot 10^{-4}$	$1.1 \cdot 10^{-7}$	1.7	0.50	[43]
$^{35}$ Cl + $^{24}$ Mg	$^{59}\mathrm{Cu}$	37	$1.1 \cdot 10^{-4}$	$1.3 \cdot 10^{-7}$	1.7	0.51	[49]
$^{32}S + ^{27}Al$	<sup>59</sup> Cu	42	$1.3 \cdot 10^{-4}$	$1.2 \cdot 10^{-7}$	2.0	0.53	[27]
$^{16}O + {}^{54}Fe$	$^{70}\mathrm{Se}$	34	$2.5 \cdot 10^{-5}$	$3.0 \cdot 10^{-8}$	1.3	0.46	[32]

TABLE III. Typical quantities of the evaporation calculations performed using the statistical-model code CACARIZO as discussed in the text. The deformability parameters are taken either from the parameter set  $\mathbf{B}$  (see Table II) for  $^{28}\mathrm{Si}$  +  $^{12}\mathrm{C}$  or from similar fitting procedures for the other systems studied in the literature.

### **FIGURES**

Figure 1: Experimental C (solid squares), N (solid triangles), and O (solid circles) cross sections measured in the <sup>28</sup>Si + <sup>12</sup>C reaction [4,5] as compared to the calculations (dotted curves) performed with the equilibrium model of orbiting [3]. The solid curves are the predictions of the transition-state model [1]. The open squares, triangles and circles are the present data of the C, N, and O fully-damped yields with error bars smaller than the size of the symbols. The full diamonds correspond to ER cross sections quoted in Refs. [6–12].

Figure 2: Inclusive energy spectra of  $\alpha$  particles measured in the <sup>28</sup>Si + <sup>12</sup>C reaction at E<sub>lab</sub> = 112 MeV (a) and (b), and 180 MeV (c) and (d) at  $\Theta_{lab}^{LCP} = 40^{\circ}$  and 45°. The experimental data are shown by the solid points with error bars visible when greater than the size of the points. The solid and dashed lines are statistical-model calculations discussed in the text.

Figure 3: Exclusive energy spectra of  $\alpha$  particles emitted at the angles  $+40^{\circ} < \Theta_{lab}^{LCP} < +65^{\circ}$ , in coincidence with individual P and S ER's detected at -15° in the <sup>28</sup>Si + <sup>12</sup>C reaction at  $E_{lab} = 112$  MeV. The experimental data are given by the solid points with error bars visible when greater than the size of the points. The solid lines are statistical-model calculations discussed in the text.

Figure 4 Exclusive energy spectra of  $\alpha$  particles emitted at the angles  $+40^{\circ} < \Theta_{lab}^{LCP} < +95^{\circ}$ , in coincidence with individual P and S ER's detected at -10° in the <sup>28</sup>Si + <sup>12</sup>C reaction at  $E_{lab} = 180$  MeV. The experimental data are given by the solid points with error bars visible when greater than the size of the points. The solid lines are statistical-model calculations discussed in the text.

Figure 5: Exclusive energy spectra of protons emitted at the angles  $+40^{\circ} < \Theta_{lab}^{LCP} < +70^{\circ}$ , in coincidence with individual P and S ER's detected at -10°, at the indicated laboratory angles, in the  $^{28}\text{Si}(180 \text{ MeV}) + ^{12}\text{C}$  reaction. The solid lines are statistical-model calculations discussed in the text.

Figure 6: In-plane angular correlations of  $\alpha$  particles (circles) and protons (triangles) measured in coincidence with the ER's Z = 16 (a) and 15 (b) in the <sup>28</sup>Si + <sup>12</sup>C reaction at  $E_{lab} = 112$  MeV in the angular range -115°  $\leq \Theta_{lab}^{LCP} \leq +115$ °). The proton correlations have been multiplied by a factor  $10^{-3}$  for the sake of clarity. The arrow indicates the position of the IC detector at  $\Theta_{lab} = -15$ °. On the abscissa, the positive angle refer to the opposite side of the beam from the direction of the ER detected in IC. The solid lines correspond to statistical-model calculations discussed in the text.

Figure 7: In-plane angular correlations of  $\alpha$  particles (circles) and protons (triangles) measured in coincidence with the ER's with Z = 17 (a), 16 (b), 15 (c), and 14 (d) in the  $^{28}$ Si +  $^{12}$ C reaction at E<sub>lab</sub> = 180 MeV. in the angular range -115°  $\leq \Theta_{lab}^{LCP} \leq +115$ °). The proton correlations have been multiplied by a factor  $10^{-2}$  for the sake of clarity. The arrow indicates the position of the IC detector at  $\Theta_{lab}$ = -10°. On the abscissa, the positive angle refer to the opposite side of the beam from the direction of the ER detected in IC. The solid lines correspond to statistical-model calculations discussed in the text.

Figure 8: Out-of-plane angular correlations of coincident  $\alpha$  particles (circles) and protons (triangles) measured in the <sup>28</sup>Si + <sup>12</sup>C reaction at  $E_{lab} = 180$  MeV. The proton correlations have been multiplied by a factor  $10^{-2}$  for the sake of clarity. The ER's with Z = 17 (a), 16 (b), 15 (c), and 14 (d) are detected at  $\Theta_{lab} = -10^{\circ}$ . The solid lines correspond to statistical-model calculations discussed in the text.

Figure 9: Energy-correlation plots between coincident  $\alpha$  particles and S ER's produced in the <sup>28</sup>Si + <sup>12</sup>C reaction at E<sub>lab</sub> = 180 MeV. The heavy fragment is detected at  $\Theta_S = -10^{\circ}$  and the  $\alpha$ -particle angle settings are given in the figure. The dashed lines correspond to different contours with their associated labellings discussed in the text.

Figure 10: Experimental (a,c) and calculated (b,d) energy-correlation plots between coincident  $\alpha$  particles and S ER's produced in the <sup>28</sup>Si + <sup>12</sup>C reaction at E<sub>lab</sub> = 180 MeV. The S is identified at  $\Theta_S = -10^{\circ}$  and the  $\alpha$  particles are detected at  $\Theta_{\alpha} = +40^{\circ}$ , and +70°, respectively. CACARIZO calculations are discussed in the text.

Figure 11: Excitation-energy spectra calculated for the  $^{28}\text{Si} + ^{12}\text{C}$  reaction at  $\text{E}_{lab} = 180$  MeV for  $^{8}\text{Be}$  (a) and  $^{32}\text{S}$  in coincidence with the g.s.(b) and first excited level (c) of  $^{8}\text{Be}$ . The solid line corresponds to the energy of the first excited state of  $^{8}\text{Be}$  (3.08 MeV). The dashed lines correspond to an excitation energy in  $^{32}\text{S}$  expected for an  $\alpha$ -transfer process. The lower spectrum in (b) corresponds to the sum of the 4 individuals spectra.